

Towards Memory Efficient Training via Dual Activation Precision

Guanchu Wang
Rice University
guanchu.wang@rice.edu

Zirui Liu
Rice University
tradigrada@tamu.edu

Zhimeng Jiang
Texas A&M University
zhimengj@tamu.edu

Ninghao Liu
University of Georgia
ninghao.liu@uga.edu

Na Zou
Texas A&M University
zou1@tamu.edu

Xia Hu
Rice University
xia.hu@rice.edu

Abstract

Activation compressed training (ACT) has been shown to be a promising way to reduce the memory consumption in training deep neural networks. However, existing work of ACT relies on searching for the optimal bit-width during deep neural network (DNN) training to reduce the quantization noise, which makes the procedure complicated and less transparent. To this end, we propose a simple and effective ACT method for DNN training. Our method is motivated by the observation: *DNN backward propagation mainly depends on the low-frequency component (LFC) of the activation maps instead of the high-frequency component (HFC)*. It indicates the HFC of the activation maps is highly redundant and compressible during DNN training, which inspires our proposed Dual ActIVation PrecISION (DIVISION). During the training, DIVISION estimates both the LFC and HFC of the activation maps, and compresses the HFC into low-precision copy to remove the redundancy. This can significantly reduce the memory consumption without negatively affecting the precision of DNN backward propagation. In this way, DIVISION achieves comparable performance as normal training. Experimental results on three benchmark datasets demonstrate that DIVISION outperforms state-of-the-art baseline methods in terms of memory consumption, model accuracy, and running speed.

1 Introduction

Deep neural networks (DNNs) have been widely applied to real-world tasks such as language understanding [1, 2], machine translation [3], visual detection and tracking [4, 5]. With increasingly larger and deeper architectures, DNNs achieve remarkable improvement in representation learning and generalization capacity [6, 7]. Generally, training a larger model requires more memory resources to cache the activation values of all intermediate layers during the back-propagation¹. For example, training a DenseNet-121 [8] on the ImageNet dataset [9] requires to cache over 1.3 billion float activation values (4.8GB) during back-propagation; and training a ResNet-50 [10] requires to cache over 4.6 billion float activation values (17GB). Some techniques have been developed to reduce the training cache of DNNs, such as checkpointing [11, 12], mix precision training [13, 14], low bit-width training [15, 16] and activation compressed training [17, 18, 19]. Among these, the activation compressed training (ACT) has emerged as a promising method due to its significant reduction of training memory and the competitive learning performance [20, 21].

¹The activation map of each layer is required for estimating the gradient in DNN training.

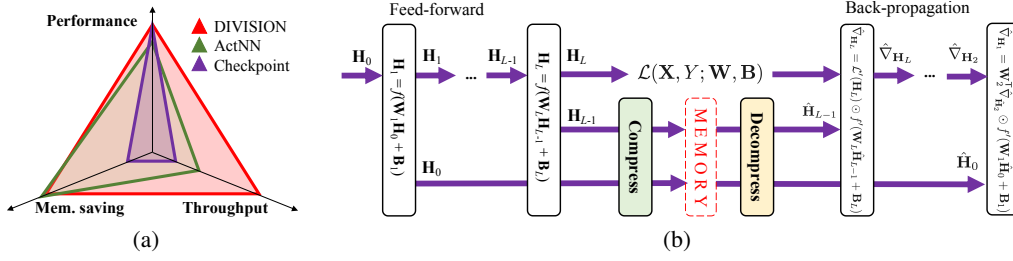


Figure 1: (a) Overall performance of DIVISION versus baseline methods. (b) Framework of activation compressed training.

Existing work of ACT relies on quantizing the activation maps to reduce the memory consumption of DNN training, such as BLPA [22], TinyScript [18] and ActNN [20]. Although ACT could significantly reduce the training memory footprint, the quantization process introduces noises in backward propagation, which makes the training suffer from undesirable performance degradation [18]. Due to this reason, BLPA requires at least 4-bit ACT to ensure the convergence of DNNs on the ImageNet dataset [22], which has only 16% (approximate value) compression of the activation maps. To solve this problem, some work proposes to search for the optimal bit-width to match different samples during training, such as ActNN [20] and AC-GC [23]. Although it can moderately reduce the quantization noise and leads to the convergence of DNNs under 2-bit ACT (nearly 10% compression rate), the following issues cannot be ignored. First, it is time-consuming to search for the bit-width during DNN training. Second, the framework of bit-width searching is complicated and non-transparent, which brings challenges to follow-up studies on the ACT and its real-world applications.

To tackle the challenge, we propose a simple and transparent method to reduce the cache of DNN training in this work. Our method is motivated by an instructive observation: *DNN backward propagation mainly depends on the low-frequency component (LFC) of the activation maps instead of the high-frequency component (HFC)*. Specifically, it is observed in our experiment: DNN training suffers from less performance degradation after removing the HFC from the activation maps of each layer, compared with removing the LFC. This indicates the LFC contains significantly more task-relevant semantic information for the backward propagation [24]. It also indicates the HFC of activation map is highly redundant and compressible during the DNN training.

Motivated by this observation, we propose Dual Activation Precision (DIVISION) to reduce the memory consumption of DNN training. Generally, the majority of memory is used for caching the HFC of activation maps. The high-level idea is to remove the redundant information in the HFC during the training. Specifically, DIVISION first estimates both the LFC and HFC from activation maps; then preserves the high-precision LFC and compresses the HFC into a light-weight copy with low numerical precision. In this way, DIVISION can significantly reduce the memory consumption. Meanwhile, it will not negatively affect the quality of backward propagation and could maintain competitive training performance.

Compared with the existing frameworks that integrate searching into learning [20, 23], DIVISION has a more efficient compressor and decompressor (purely feed-forward and parallelizable). Moreover, it demonstrates that DNN backward propagation focuses more on the LFC of activation maps, while an approximated version of HFC is enough. Experiments are conducted to evaluate DIVISION in terms of the memory consumption, training performance, and running speed. A qualitative comparison is given in Figure 1 (a). Our proposed DIVISION consistently outperforms state-of-the-art baseline methods in the above three aspects. The contributions of this work are summarized as follows:

- We experimentally demonstrate that DNN backward propagation mainly focuses on the LFC of the activation maps instead of the HFC.
- Following this direction, we propose DIVISION to reduce the redundancy of the HFC of the activation maps in order to reduce the cache of DNN training.
- Experiments on three benchmark datasets demonstrate the effectiveness of DIVISION in terms of memory consumption, training performance, and running speed.

2 Preliminary

2.1 Notations

Without loss of generality, we consider an L -layer deep neural network in this work. For each layer l ($1 \leq l \leq L$), the activation map during the forward pass is calculated by

$$\mathbf{H}_l = f(\mathbf{W}_l \mathbf{H}_{l-1} + \mathbf{B}_l), \quad (1)$$

where \mathbf{H}_l denotes the activation map of layer l ; \mathbf{H}_0 takes a mini-batch of input images; \mathbf{W}_l and \mathbf{B}_l denote the weight and bias of layer l , respectively; and $f(\cdot)$ denotes the activation function.

2.2 Activation Compressed Training

It has been proved in existing work [16] that majority of memory consumption (nearly 90%) is for the storage of the activation maps in DNN training. The activation compressed training (ACT) solves this problem via real-time compressing and reconstructing the activation maps during the training process. A typical ACT framework in existing work [22] is shown in Figure 1 (b). Specifically, after the feed-forward pass of each layer l , ACT compresses the activation map \mathbf{H}_l and caches the representation to the memory. The compression enables a significant reduction of memory compared with caching the original (exact) activation maps. During the backward pass of each layer l , ACT decompresses the cached representation into the recovered activation maps $\hat{\mathbf{H}}_l$, which are used for estimating the gradient and updating the parameters. Formally, the gradient of the loss value towards the weight $\hat{\nabla}_{\mathbf{W}_l}$, bias $\hat{\nabla}_{\mathbf{B}_l}$, and activation map $\hat{\nabla}_{\mathbf{H}_l}$ is estimated by

$$\begin{aligned} \hat{\nabla}_{\mathbf{W}_l} &= \hat{\nabla}_{\mathbf{H}_l} \odot f'(\mathbf{W}_l \hat{\mathbf{H}}_{l-1} + \mathbf{B}_l) \hat{\mathbf{H}}_{l-1}^T, \\ \hat{\nabla}_{\mathbf{B}_l} &= \hat{\nabla}_{\mathbf{H}_l} \odot f'(\mathbf{W}_l \hat{\mathbf{H}}_{l-1} + \mathbf{B}_l), \\ \hat{\nabla}_{\mathbf{H}_{l-1}} &= \mathbf{W}_l^T \hat{\nabla}_{\mathbf{H}_l} \odot f'(\mathbf{W}_l \hat{\mathbf{H}}_{l-1} + \mathbf{B}_l), \end{aligned} \quad (2)$$

where $\hat{\mathbf{H}}_l$ denotes the reconstructed value of \mathbf{H}_l after the decompression; \odot denotes element-wise production; and $f'(\cdot)$ denotes the derivative of the activation function.

Even though the compression of activation maps is lossy, i.e. $\hat{\mathbf{H}}_l \neq \mathbf{H}_l$ for $1 \leq l \leq L$. It has been proved ACT can limit the reconstruction error flowing back to early layers and enables the training to approach an approximately optimal solution [20].

2.3 Discrete Cosine Transformation

Discrete Cosine Transformation (DCT) projects the target data from the space domain to the frequency domain via the inner-production of the signal and a collection of cosine functions with different frequency [25]. We focus on the 2D-DCT in this work, where the target data is the input image and activation maps of DNNs. Specifically, for a $N \times N$ image or activation map \mathbf{H} , the frequency-domain feature $\tilde{\mathbf{H}}$ is estimated by $\tilde{\mathbf{H}} = \mathcal{DCT}(\mathbf{H})^2$, where $\tilde{\mathbf{H}}$ is also in the shape of $N \times N$; and each of the element $\tilde{h}_{i,j}$ is given by

$$\tilde{h}_{i,j} = \sum_{m=0}^{N-1} \sum_{n=0}^{N-1} h_{m,n} \cos \left[\frac{\pi}{N} \left(m + \frac{1}{2} \right) i \right] \cos \left[\frac{\pi}{N} \left(n + \frac{1}{2} \right) j \right], \quad (3)$$

where $h_{m,n}$, $0 \leq m, n \leq N-1$, are elements in the original activation map. Different from a single image, a feature map of DNNs is in the shape $Mini\text{-}batch \times Channel \times N \times N$. In this case, the frequency-domain feature is estimated via operating 2D-DCT for each $N \times N$ matrix repetitively.

With DCT, we could extract the low-frequency/high-frequency component (LFC/HFC) of an image, using a pipeline of low-pass/high-pass masking and inverse DCT, as shown in Figure 2. To be concrete, the estimation of LFC and HFC is given by

$$\mathbf{H}^L = i\mathcal{DCT}(\tilde{\mathbf{H}} \odot \mathbf{M}) \quad (4)$$

$$\mathbf{H}^H = i\mathcal{DCT}(\tilde{\mathbf{H}} \odot (\mathbf{1}_{N \times N} - \mathbf{M})), \quad (5)$$

²2D-DCT is operated for the 2D-feature map in each channel.

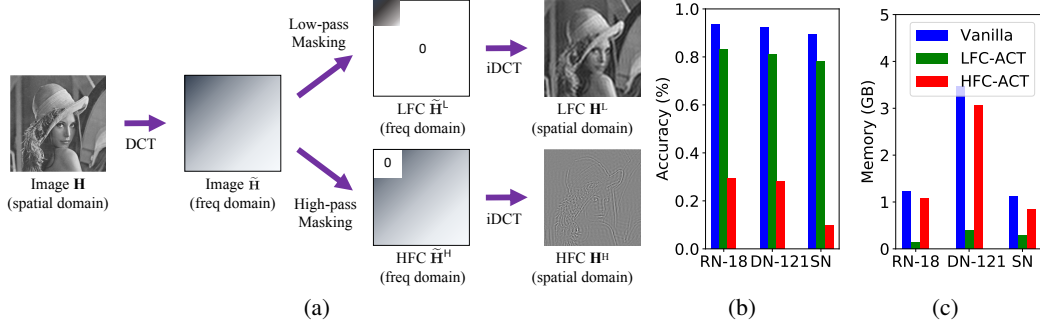


Figure 2: (a) Adopting DCT to estimate the low frequency component (LFC) and high frequency component (HFC) of an image. (b) Validation Accuracy and (c) Memory consumption of vanilla training, LFC-ACT and HFC-ACT, where RN-18, DN-121, and SN refer to the ResNet-18, DenseNet-121, and ShuffleNet-V2, respectively.

where $iDCT(\bullet)$ denotes the inverse DCT [25]; $M = [m_{i,j} | 1 \leq i, j \leq M]$ denotes a $N \times N$ low-pass mask satisfying $m_{i,j} = 1$ for $1 \leq i, j \leq W$ and $m_{i,j} = 0$ for other elements; and $1_{N \times N} - M$ indicates the high-pass mask.

3 Contribution of LFC and HFC to Backward Propagation

In this section, we experimentally investigate how the LFC and HFC activation maps contribute to the backward propagation during DNN training. Specifically, we consider three different methods to train DNNs: (M1) in vanilla training, we take the exact value of activation map H_l into Equation (2) for the backward propagation. (M2) In *LFC-ACT*, the reconstructed activation map \tilde{H}_l in Equation (2) takes the value of the LFC, $\tilde{H}_l = H_l^L$. (M3) In *HFC-ACT*, the reconstructed activation map \tilde{H}_l in Equation (2) takes the value of the HFC, $\tilde{H}_l = H_l^H$, where the LFC H_l^L and HFC H_l^H can be estimated according to Equations (4) and Equation (5), respectively.

The validation accuracy and training memory consumption of the vanilla training, LFC-ACT, and HFC-ACT on the CIFAR-10 dataset are shown in Figure 2 (b) and (c), respectively. The implementation details are given in Appendix C. Generally, we have the following observations according to the experiment results:

- According to Figure 2 (a) and (b), backward propagation without LFC of activation maps suffers from significantly more degradation of validation accuracy than without the HFC. i.e. the training performance mainly relies on the LFC of activation maps.
- According to Figure 2 (c), the storage of HFC requires significantly more memory than that of the LFC. i.e. The storage of HFC consumes the majority of memory.

Note that the HFC of activation maps requires more memory to store but has less contribution to the backward propagation. This indicates the HFC of activation maps is highly redundant and compressible during DNN training. Motivated by this, we propose *DIVISION* to compress the activation maps using dual precisions: high-precision for the LFC and low-precision for the HFC. On the one hand, both LFC and low-precision LFC requires much less memory to cache. On the other hand, removing the redundancy of HFC will not cause the perturbation of backward propagation. In such a manner, *DIVISION* enables effective compression of training memory without degradation of training performance.

4 Dual Activation Precision Training

We introduce the proposed *Dual ActIVation PrecISION* (*DIVISION*) in this section. The framework of *DIVISION* is shown in Figure 3. Specifically, after the feed-forward operation of each layer, *DIVISION* estimates the LFC and compresses the HFC into a low-precision version such that the total memory cost is significantly decreased after the compression. Before the backward propagation

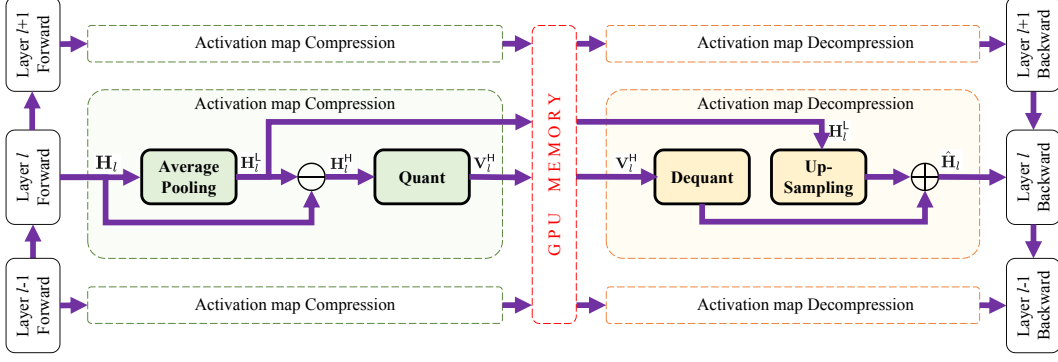


Figure 3: Framework of Dual Activation Precision Training.

of each layer, the low-precision HFC is decompressed and combined with LFC to reconstruct the activation map. The detailed compression and decompression are given as follows.

4.1 Activation Map Compression

For compressing the activation map \mathbf{H}_l of layer l , DIVISION estimates the LFC \mathbf{H}_l^L and HFC \mathbf{H}_l^H of the activation map after the feed-forward pass. However, the high computational complexity of DCT prevents us from directly applying it to real-time algorithms. We thus give Theorem 1 to introduce a moving average operation that can approximate the loss-pass filter. The proof is given in Appendix A.

Theorem 1. For any real-valued function $f(x)$ and its moving average $\bar{f}(x) = \frac{1}{2B} \int_x^{x+2B} f(t)dt$, let $F(\omega)$ and $\bar{F}(\omega)$ denote the Fourier transformation of $f(x)$ and $\bar{f}(x)$, respectively. Generally, we have $\bar{F}(\omega) = H(\omega)F(\omega)$, where $|H(\omega)| = \left| \frac{\sin \omega B}{\omega B} \right|$; and i denotes the imaginary unit.

Remark 1. The frequency response of $H(\omega)$ depends on its envelope function $\frac{1}{|\omega B|}$. Note that $\frac{1}{|\omega B|}$ decreases with $|\omega|$ such that $\frac{1}{|\omega B|} \rightarrow 0$ as $\omega \rightarrow \infty$. Hence, $H(\omega)$ is an approximate loss-pass filter.

According to Remark 1, the LFC \mathbf{H}_l^L can be approximately estimated via the moving average of \mathbf{H}_l . Note that the average pooling operator provides an efficient estimation of the moving average. DIVISION adopts the average pooling to estimate the LFC $\mathbf{H}_l^L = \text{AveragePooling}(\mathbf{H}_l)$, where the value of block-size and moving stride is a unified hyper-parameter B . B controls the memory consumption of LFC due to the fact that \mathbf{H}_l^L has N^2/B^2 elements for being cached after the compression. In our experiments, we found $B = 8$ can provide representative LFC for backward propagation, where the memory cost of LFC is only 1.6% of the original activation maps.

To estimate the HFC, DIVISION calculates the residual value $\mathbf{H}_l^H = \mathbf{H}_l - \text{UpSampling}(\mathbf{H}_l^L)$, where the up-sampling enlarge \mathbf{H}_l^L to shape $N \times N$ via nearest interpolation. Note that the LFC plays a more important role than HFC during the backward propagation. DIVISION caches the *exact* copy of LFC and *low-precision* copy of HFC, such that the total memory cost of LFC and HFC is far less than that of activation maps. To achieve the low-precision copy of HFC, DIVISION adopts Q -bit quantization³, where the bit-width Q controls the memory cost of HFC. To be concrete, let \mathbf{V}_l^H denotes a Q -bit integer matrix, as the low-precision representation of \mathbf{H}_l^H . The detailed procedure of compressing \mathbf{H}_l^H into \mathbf{V}_l^H is given by

$$\mathbf{V}_l^H = \text{Quant}(\mathbf{H}_l^H) = \lfloor \Delta_l^{-1}(\mathbf{H}_l^H - \delta_l) \rfloor, \quad (6)$$

where δ_l denotes the minimum element in \mathbf{H}_l^H ; $\Delta_l = (h_{\max} - \delta_l)/(2^Q - 1)$ denotes the quantization step; h_{\max} denotes the maximum element in \mathbf{H}_l^H ; and $\lfloor \bullet \rfloor$ denotes the *stochastic rounding*^{4,5} [26]. In this way, the memory of \mathbf{V}_l^H is $N^2Q/8$ Bytes, in contrast with that of \mathbf{H}_l being $4N^2$ Bytes. In our

³For maximizing the efficiency of data processing, DIVISION adopts a unified bit-width for all layers.

⁴ $\lfloor x \rfloor$ takes the value of $\lfloor x \rfloor$ with a probability of $x - \lfloor x \rfloor$ and takes $\lfloor x \rfloor + 1$ with a probability of $\lceil x \rceil - x$.

⁵The stochastic rounding enables the quantization-dequantization pipeline to be unbiased, i.e. $\mathbb{E}[\mathbf{V}_l^H] = \mathbf{H}_l^H$.

experiments, we found $Q=2$ can provide enough representation for backward propagation, where the memory cost of HFC is only 6.25% of the original activation maps.

After the compression, as the representation of \mathbf{H}_l , the tuple of $(\mathbf{H}_l^L, \mathbf{V}_l^H, \Delta_l, \delta_l)$ is cached to the memory for reconstructing the activation maps during the backward pass.

4.2 Activation Map Decompression

During the backward pass, the tuple of $(\mathbf{H}_l^L, \mathbf{V}_l^H, \Delta_l, \delta_l)$ is adopted to reconstruct the activation map of layer l . Specifically, the HFC is dequantized via $\hat{\mathbf{H}}_l^H = \Delta_l \mathbf{V}_l^H + \delta_l$, which is the inverse process of Equation (6). Then, the activation map is reconstructed via

$$\hat{\mathbf{H}}_l = \text{UpSampling}(\mathbf{H}_l^L) + \hat{\mathbf{H}}_l^H, \quad (7)$$

where the up-sampling enlarge \mathbf{H}_l^L to shape $N \times N$ via nearest interpolation. After the decompression, DIVISION takes the value of $\hat{\mathbf{H}}_l$ into Equation (2) to estimate the gradient $\hat{\nabla}_{\mathbf{W}_l}$, $\hat{\nabla}_{\mathbf{B}_l}$ and $\hat{\nabla}_{\mathbf{H}_{l-1}}$.

4.3 Theoretical Compression Rate of DIVISION

For each layer l of DNNs, DIVISION requires approximate $(4B^{-2} + Q/8)N^2$ Bytes memory to cache the tuple of $(\mathbf{H}_l^L, \mathbf{V}_l^H, \Delta_l, \delta_l)$ after the compression. In contrast, the vanilla training requires $4N^2$ Bytes memory to cache the activation map \mathbf{H}_l . In this way, DIVISION has the compression rate of memory given by $(B^{-2} + Q/32)^{-1}$, where B and Q are the hyper-parameters to control the compression rate. To be more concrete, B denotes the block-size of average pooling and Q denotes the bit-width of quantization. The detailed derivation of compression rate is given in Appendix B. In our experiment, we found $B=8$ and $Q=2$ can provide loss-less training performance, where the theoretical compression rate is $12.8\times$ of vanilla training. The practical compression rate should be slightly higher than the theoretical value due to other caches during the training.

4.4 Algorithm of DIVISION

Algorithm 1 demonstrates a mini-batch updating of DIVISION. To be concrete, the updating of each layer l includes the forward pass and backward pass. During the forward pass, DIVISION first calculates the exact activation map for forwarding to the next layer (line 2); then, estimates the LFC and HFC (line 3-4); after this, achieves the low precision copy of HFC (lines 5); finally caches the representation to the memory (line 6). During the backward pass, DIVISION first decompresses the HFC (line 10); then reconstructs the activation map (line 11); after this, updates the weights and bias of layer l via stochastic gradient descent (line 12-13); finally frees the caching of $(\mathbf{H}_l^L, \mathbf{V}_l^H, \Delta_l, \delta_l)$ (line 14). For each mini-batch updating, the memory usage reaches the maximum value (caching of activation maps, dataset and optimizer) after the forward pass, and reduces to the minimum value (caching of dataset and optimizer) after the backward pass.

Algorithm 1 Mini-batch updating of DIVISION

Input: Mini-batch samples \mathbf{x} and labels \mathbf{y} .

Output: Weight and bias $\{\mathbf{W}_l, \mathbf{B}_l | 1 \leq l \leq L\}$.

```

1: for layer  $l := 0$  to  $L-1$  do
2:    $\mathbf{H}_{l+1} = f(\mathbf{W}_l \mathbf{H}_l + \mathbf{B}_l) // \mathbf{H}_0 = \mathbf{x}$ 
3:    $\mathbf{H}_l^L = \text{AveragePooling}(\mathbf{H}_l)$ 
4:    $\mathbf{H}_l^H = \mathbf{H}_l - \mathbf{H}_l^L$ 
5:    $\mathbf{V}_l^H, \Delta_l, \delta_l = \text{Quant}(\mathbf{H}_l^H)$ 
6:   Cache  $(\mathbf{H}_l^L, \mathbf{V}_l^H, \Delta_l, \delta_l)$  to the memory.
7: end for
8: Estimate the Loss value and the gradient  $\hat{\nabla}_{\mathbf{H}_L}$ .
9: for layer  $l := L-1$  to  $0$  do
10:   $\hat{\mathbf{H}}_l^H = \text{Dequant}(\mathbf{V}_l^H, \Delta_l, \delta_l)$ 
11:   $\hat{\mathbf{H}}_l = \text{UpSampling}(\mathbf{H}_l^L) + \hat{\mathbf{H}}_l^H$ 
12:  Estimate  $\hat{\nabla}_{\mathbf{W}_{l+1}}, \hat{\nabla}_{\mathbf{B}_{l+1}}$  and  $\hat{\nabla}_{\mathbf{H}_l}$  by Eq.(2).
13:  Update the value of  $\mathbf{W}_{l+1}$  and  $\mathbf{B}_{l+1}$ .
14:  Free the caching of  $(\mathbf{H}_l^L, \mathbf{V}_l^H, \Delta_l, \delta_l)$ .
15: end for
```

5 Experiments

We conduct the experiments to evaluate DIVISION in terms of the training performance, memory consumption, and running speed.

5.1 Experiment Setting

Datasets. We consider CIFAR-10, CIFAR-100 [27] and ImageNet-1K [9] datasets in our experiments. **CIFAR-10:** An image dataset with 60,000 color images in 10 different classes, where each image has 32×32 pixels. **CIFAR-100:** An image dataset with 60,000 color images in 100 different classes, where each image has 32×32 pixels. **ImageNet:** A large scale image dataset which has over one million color images covering 1000 categories, where each image has 224×224 pixels.

Baseline Methods. **Vanilla:** Training with high-precision activation map during the forward and backward pass. **BLPA:** A systemic implementation of ACT by [22], which only supports ResNet-related architectures. **AC-GC:** A framework of ACT with automatic searched bit-width for the quantization of activation maps [23]. **ActNN:** Activation compression training with dynamic bit-width quantization, where the bit-allocation minimizes the variance of activation maps via dynamic processing [20]. For all ACT methods, the activation maps of the input layer and inter-media layers are compressed during the training, that of the final layer is not compressed due to its terribly impact on the estimation of loss value. This has been proved effective in existing work [22]. **Checkpoint:** Releasing the inter-media activation maps to reduce the memory consumption, and replaying parts of the forward pass to reconstruct the activation map during the backward pass [11]. **SWAP:** Swapping the activation maps to the CPU during the forward pass the memory consumption of GPU, and reload the activation maps to GPU during the backward pass [28].

Applied Model Architectures. For the evaluation of training performance, we consider ResNet-18 (top1 accuracy 94.89%) and ResNet-164 (top1 accuracy 94.9%) on the CIFAR-10 dataset; DenseNet-121 (top1 accuracy 79.75%) and ResNet-164 (top1 accuracy 77.3%) on the CIFAR-100 dataset; and ResNet-50 (top1 accuracy 76.15%) as well as DenseNet-161 (top1 accuracy 77.65%) on the ImageNet dataset. Our reproduced validating accuracy is consistent with the official results of torchvision⁶. Moreover, for the evaluation of memory consumption and training throughput, we consider the larger models ResNet-50 and WRN-50-2 on the ImageNet dataset. The CIFAR datasets are too tiny to be involved in the evaluation of memory and throughput.

5.2 Evaluation by Model Accuracy

In this section, we evaluate the training methods in terms of model accuracy. Specifically, DIVISION is compared with BLPA [22], AC-GC [23] and ActNN [20]. The configuration (including the hyper-parameters) of DIVISION and baseline methods are given in Appendix C and D, respectively. Here, Checkpoint and SWAP are not considered in this section because they are able to reduce the training memory without degradation of model accuracy. The top-1 validating accuracy on the CIFAR-10, CIFAR-100 and ImageNet datasets is given in Table 1. We have the following observations:

- **DIV. vs Baselines:** Compared with the vanilla training, DIVISION achieves nearly loss-less validation accuracy (less than 0.3%) on the three datasets. Regarding the ACT methods, BLPA and AC-GC need a higher compression rate than DIVISION, and ActNN has nearly the same level of compression rate. However, the baseline methods suffer from slightly higher validation error on the ImageNet dataset, which demonstrates the effectiveness of DIVISION.
- **Accuracy & Simplicity of DIV.:** ActNN relies on dynamic programming to optimize the bit-width and adopt non-unified quantization towards different operators and training instances. Dynamic programming is with high computational complexity and cannot be optimized with parallel structure. In contrast, DIVISION adopts the average pooling and unified quantization for the compression, which is more concise without loss of effectiveness.
- **Compressibility of HFC:** Note that DIVISION adopts relatively lower compression rate (2/32) for the HFC of activation map during the training, but achieves nearly loss-less accuracy. This result indicates the HFC of activation map is highly redundant and compressible to the training of DNNs.

5.3 Evaluation by Memory Consumption

We evaluate the training methods by measuring their memory cost on the ImageNet dataset. Specifically, during the training of DNNs, the activation maps are stored layer-by-layer in the forward

⁶<https://paperswithcode.com/lib/torchvision>

	Architecture	Vanilla	BLPA	AC-GC	ActNN-L3	DIVISION
CIFAR-10	ResNet-18	94.89	-	90.43	94.84	94.62
	ResNet-164	94.90	94.51	-	-	94.58
CIFAR-100		77.3	76.42	73.37	-	76.70
	DenseNet-121	79.75	-	-	78.95	79.64
ImageNet	ResNet-50	76.15	-	72.7	75.42	76.12
	DenseNet-161	77.65	-	-	76.59	77.55

Table 1: Top-1 validation accuracy (%) \uparrow of DIVISION compared with the baseline methods.

pass, and freed layer-by-layer (in reverse order) in the backward propagation. In such a manner, the memory utilization increases to peak value after a forward pass, and reduces to the minimum after the backward propagation [22]. Therefore, the memory overhead of a training DNNs can be estimated by

$$\text{Memory Cost} = \text{Memory Utilization}_{\text{after forward}} - \text{Memory Utilization}_{\text{after backward}}, \quad (8)$$

where existing deep learning tools provide APIs⁷ to estimate the memory utilization.

The training mini-batchsize is selected from $\{64, 128, 256, 512\}$ since the vanilla method will run out of memory when the mini-batchsize > 512 . The configuration of DIVISION, baseline methods and our computational infrastructure are given in Appendix C, D and E, respectively. Table 2 gives the memory consumption by all methods, where the normalized consumption (in percentage) by each method is estimated via taking the consumption value of vanilla training as the baseline. Overall, we have the following observations:

- **DIV. vs SWAP:** SWAP contributes to reducing the GPU memory overhead merely by the transfer the overhead from GPU to CPU, which is non-effective if considering the memory utilization of both GPU and CPU. Therefore, SWAP is limited by the capacity of CPU, and becomes out of memory when the mini-batch size ≥ 512 in training ResNet-50, and mini-batch size ≥ 256 in training WRN-50-2 according to Table 2.
- **DIV. vs Checkpoint:** Checkpoint suffers from the memory-speed trade-off, and shows considerable memory overhead compared with DIVISION. This is because it relies on replaying the forward pass of the layers without cached activation map for backward propagation.
- **DIV. vs BLPA:** DIVISION is with significantly lower memory overhead compared with BLPA. This is because BLPA relies on at least 4-bit ACT to achieve the convergence of training, leading to its compression rate higher than DIVISION.
- **DIV. vs AC-GC:** The practical memory cost of AC-GC should be greater than the values given in Table 2. AC-GC searches the bit-width from an initial maximum value, and finalizes with an optimal bit-width. Thus, the average memory cost should be greater than that in the last epoch.
- **DIV. vs ActNN:** DIVISION is with the same level of memory overhead compared with ActNN. Although DIVISION needs slightly extra memory to cache the LFC of activation maps. This extra overhead is negligible (only 1% of vanilla training).
- **Activation Maps:** For the vanilla training, the majority of memory utilization is for the storage of activation maps (nearly 90%, and even growing with the mini-batch size), which is consistent with our discussion in Section 1.

5.4 Evaluation by Training Throughput

We now evaluate different methods in terms of the training throughput. Generally, the throughput indicates the running speed of a training method via the counting the average number of data samples processed per second. The throughput is given by $\frac{\text{Mini-batch Size}}{T_{\text{batch}}}$, where T_{batch} denotes the time consumption of updating a mini-batch of samples. Each method is combined with the automatic mixed precision (AMP)⁸ to improve the training throughput, which is estimated based on 100 times

⁷`torch.cuda.memory_allocated` returns the memory occupied by tensors in bytes for a target device.

⁸<https://pytorch.org/docs/stable/amp.html>

Architecture		ResNet-50				WRN-50-2			
Batch-size		64	128	256	512	64	128	256	512
Total. Mem (GB)	Vanilla	5.46	10.62	20.92	OOM	7.52	14.23	27.68	OOM
	SWAP (CPU+GPU)	5.46 100%	10.62 100%	20.92 100%	OOM	7.52 100%	14.23 100%	OOM	OOM
	Checkpoint	1.23 22.5%	2.16 20.3%	4.03 19.3%	7.76	1.71 22.7%	2.65 18.6%	4.51 16.3%	8.25
	BLPA	1.18 21.6%	2.01 18.9%	3.67 17.5%	6.99	1.87 24.9%	2.96 20.8%	5.15 18.6%	9.51
	AC-GC	1.8 33.0%	3.31 31.2%	6.31 30.2%	12.33	2.72 36.2%	4.66 32.8%	8.53 30.8%	16.27
	ActNN-L3	0.81 14.8%	1.34 12.6%	2.39 11.4%	4.47	1.44 19.1%	2.09 14.7%	3.41 12.3%	6.03
	DIVISION	0.87 15.9%	1.4 13.2%	2.6 12.4%	4.89	1.51 20.1%	2.24 15.7%	3.68 13.3%	6.58
Act. Mem (GB)	Vanilla	5.14	10.25	20.48	OOM	6.7	13.38	26.75	OOM
	SWAP (CPU)	5.14 100%	10.25 100%	20.48 100%	OOM	6.7 100%	13.38 100%	OOM	OOM
	Checkpoint	0.9 17.5%	1.8 17.6%	3.59 17.5%	7.18	0.9 13.4%	1.8 13.5%	3.59 13.4%	7.18
	BLPA	0.85 16.5%	1.64 16%	3.23 15.8%	6.41	1.06 15.8%	2.11 15.8%	4.22 15.8%	8.44
	AC-GC	1.47 28.6%	2.94 28.7%	5.88 28.7%	11.75	1.91 28.5%	3.81 28.5%	7.61 28.4%	15.2
	ActNN-L3	0.49 9.5%	0.97 9.5%	1.95 9.5%	3.89	0.62 9.3%	1.25 9.3%	2.49 9.3%	4.97
	DIVISION	0.54 10.5%	1.08 10.5%	2.16 10.5%	4.31	0.69 10.3%	1.39 10.4%	2.76 10.3%	5.51

Table 2: Memory consumption ↓ and compression rate ↑ of different methods. *Total. Mem.* refers to the overall memory consumption including that of parameters, input image, optimizer and activation maps. *Act. Mem.* refers to the memory consumption of the activation map of all layers except the final layer. *OOM* refers to out of memory.

of mini-batch updating on the ImageNet dataset. The average throughput of DNN training is given in Figure 4. Overall, we have the following observations:

- **Vanilla Training:** The vanilla method is faster as a result of no compression or reconstruction of the activation maps during the forward and backward process. However, the significant memory overhead leads to the out-of-memory issue when the mini-batch size is 512.
- **Reason for Time overhead:** Compared with the vanilla method, the time overhead of DIVISION comes from the computation of LFC and compression of HFC. In ActNN, the overhead mainly comes from the the dynamic bit-width allocation and activation map quantization. In Checkpoint, it comes from replaying the forward process of inter-media layers. In SWAP, the overhead mainly derives from the communication cost between the CPUs and GPUs.
- **DIV. vs Vanilla:** DIVISION has nearly 1/4 degradation of the throughput compared with the vanilla training, which is more efficient than the remaining baseline methods.
- **DIV. vs ActNN:** Compared with DIVISION, the dynamic bit-width allocation in ActNN leads to high computational overhead which cannot be parallelized. In contrast, the mean filtering in DIVISION is efficient operation (average pooling) for deep learning.
- **DIV. vs Checkpoint & SWAP:** Checkpoint and SWAP are less efficient than ACT-based methods (DIVISION and ActNN). This indicates the replaying cost of inter-media layers and communication cost of CPU-GPU are larger than the cost of processing the activation maps.

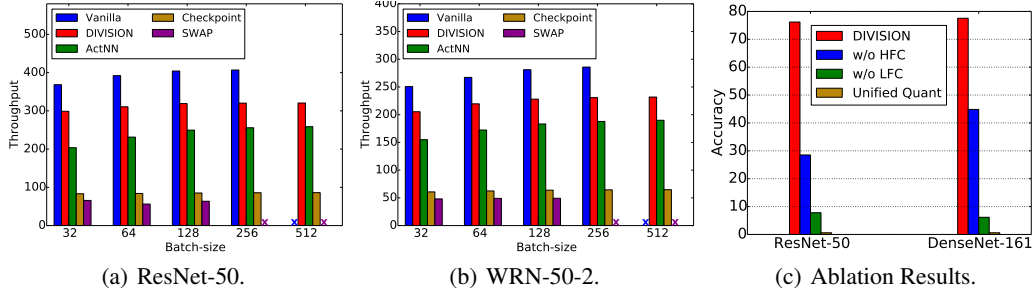


Figure 4: Training throughput \uparrow of (a) Resnet-50 and (b) WRN-50-2 on the ImageNet dataset, where \times indicates out of memory. (c) Model accuracy (%) \uparrow of DIVISION, DIVISION w/o HFC, DIVISION w/o LFC and Unified quantization on the ImageNet dataset.

5.5 Ablation Study (RQ4)

Both the LFC and HFC of the activation maps contribute to DNN backward propagation. To prove this, we conduct experiments on the ImageNet dataset to compare DIVISION with three variants: **DIVISION w/o HFC**: Caching the LFC of the activation maps for the reconstruction. **DIVISION w/o LFC**: Caching the HFC for the reconstruction. **Unified quant.**: Quantizing the activation maps without splitting in the frequency domain. In the ablation experiment, DIVISION w/o HFC takes block-size $B = 4$ for the filter of LFC; DIVISION w/o LFC takes the bit-width $Q = 2$ for the quantization of HFC; DIVISION adopts the combination of these settings for dual precision compression; and the unified quant. follows the DIVISION w/o LFC to have 2-bit quantization as well. The top-1 validation accuracy of different methods are given in Figure 4 (c). Overall, we have the following observations:

- **Necessity of LFC and HFC**: DIVISION outperforms the DIVISION w/o HFC and DIVISION w/o LFC methods, where DIVISION w/o HFC converges to a low level of accuracy, and DIVISION w/o LFC even fails to converge. This indicates both HFC and LFC of activation maps provides key information for DNN backward propagation.
- **Benefits of Dual Precision**: DIVISION outperforms the Unified quant. method. This indicates the unified quantization of activation maps cannot provide enough for backward propagation. DIVISION achieves loss-less training performance via dual precision compression.
- **LFC vs HFC**: DIVISION w/o HFC outperforms the DIVISION w/o LFC method. This is consistent with our observations in the preliminary experiment: *LFC provides more semantic information for DNN backward propagation*. This also indicates the advantage of DIVISION which adopts dual precision to cache the activation map maximize the information reservation.

6 Conclusion

In this work, we discover a novel phenomenon in DNN training: the LFC of activation maps provides most of the semantic information for DNN backward propagation, while the HFC is highly redundant and compressible. Motivated by this, we propose DIVISION to adopt dual-precision activation maps for DNN backward propagation: high-precision for LFC and low-precision for HFC. Experiments on three benchmark datasets demonstrate DIVISION significantly reduces the training memory consumption, and achieves lossless training performance. This indicates the high-precision LFC combined with low-precision HFC can provide sufficient information for DNN backward propagation. Moreover, DIVISION never relies on dynamic programming to reduce the quantization noise during the training. This enables DIVISION to be more efficient, and achieves higher training throughput than baseline methods.

References

- [1] Jacob Devlin, Ming-Wei Chang, Kenton Lee, and Kristina Toutanova. Bert: Pre-training of deep bidirectional transformers for language understanding. *arXiv preprint arXiv:1810.04805*,

- 2018.
- [2] William Fedus, Barret Zoph, and Noam Shazeer. Switch transformers: Scaling to trillion parameter models with simple and efficient sparsity. *arXiv preprint arXiv:2101.03961*, 2021.
 - [3] Ashish Vaswani, Noam Shazeer, Niki Parmar, Jakob Uszkoreit, Llion Jones, Aidan N Gomez, Łukasz Kaiser, and Illia Polosukhin. Attention is all you need. *Advances in neural information processing systems*, 30, 2017.
 - [4] Ross Girshick. Fast r-cnn. In *Proceedings of the IEEE international conference on computer vision*, pages 1440–1448, 2015.
 - [5] Joseph Redmon, Santosh Divvala, Ross Girshick, and Ali Farhadi. You only look once: Unified, real-time object detection. In *Proceedings of the IEEE conference on computer vision and pattern recognition*, pages 779–788, 2016.
 - [6] Alex Krizhevsky, Ilya Sutskever, and Geoffrey E Hinton. Imagenet classification with deep convolutional neural networks. *Advances in neural information processing systems*, 25, 2012.
 - [7] Karen Simonyan and Andrew Zisserman. Very deep convolutional networks for large-scale image recognition. *arXiv preprint arXiv:1409.1556*, 2014.
 - [8] Gao Huang, Zhuang Liu, Laurens Van Der Maaten, and Kilian Q Weinberger. Densely connected convolutional networks. In *Proceedings of the IEEE conference on computer vision and pattern recognition*, pages 4700–4708, 2017.
 - [9] Jia Deng, Wei Dong, Richard Socher, Li-Jia Li, Kai Li, and Li Fei-Fei. Imagenet: A large-scale hierarchical image database. In *2009 IEEE conference on computer vision and pattern recognition*, pages 248–255. Ieee, 2009.
 - [10] Kaiming He, Xiangyu Zhang, Shaoqing Ren, and Jian Sun. Deep residual learning for image recognition. In *Proceedings of the IEEE conference on computer vision and pattern recognition*, pages 770–778, 2016.
 - [11] Tianqi Chen, Bing Xu, Chiyuan Zhang, and Carlos Guestrin. Training deep nets with sublinear memory cost. *arXiv preprint arXiv:1604.06174*, 2016.
 - [12] Audrunas Gruslys, Rémi Munos, Ivo Danihelka, Marc Lanctot, and Alex Graves. Memory-efficient backpropagation through time. *Advances in Neural Information Processing Systems*, 29, 2016.
 - [13] Han Vanholder. Efficient inference with tensorrt. In *GPU Technology Conference*, volume 1, page 2, 2016.
 - [14] Paulius Micikevicius, Sharan Narang, Jonah Alben, Gregory Diamos, Erich Elsen, David Garcia, Boris Ginsburg, Michael Houston, Oleksii Kuchaiev, Ganesh Venkatesh, et al. Mixed precision training. *arXiv preprint arXiv:1710.03740*, 2017.
 - [15] Xiaofan Lin, Cong Zhao, and Wei Pan. Towards accurate binary convolutional neural network. *Advances in neural information processing systems*, 30, 2017.
 - [16] Jianfei Chen, Yu Gai, Zhewei Yao, Michael W Mahoney, and Joseph E Gonzalez. A statistical framework for low-bitwidth training of deep neural networks. *Advances in Neural Information Processing Systems*, 33:883–894, 2020.
 - [17] Georgios Georgiadis. Accelerating convolutional neural networks via activation map compression. In *Proceedings of the IEEE/CVF Conference on Computer Vision and Pattern Recognition*, pages 7085–7095, 2019.
 - [18] Fangcheng Fu, Yuzheng Hu, Yihan He, Jiawei Jiang, Yingxia Shao, Ce Zhang, and Bin Cui. Don’t waste your bits! squeeze activations and gradients for deep neural networks via tinscript. In *International Conference on Machine Learning*, pages 3304–3314. PMLR, 2020.
 - [19] Xiaoxuan Liu, Lianmin Zheng, Dequan Wang, Yukuo Cen, Weize Chen, Xu Han, Jianfei Chen, Zhiyuan Liu, Jie Tang, Joey Gonzalez, et al. Gact: Activation compressed training for general architectures. *arXiv preprint arXiv:2206.11357*, 2022.
 - [20] Jianfei Chen, Lianmin Zheng, Zhewei Yao, Dequan Wang, Ion Stoica, Michael Mahoney, and Joseph Gonzalez. Actnn: Reducing training memory footprint via 2-bit activation compressed training. In *International Conference on Machine Learning*, pages 1803–1813. PMLR, 2021.

- [21] Zirui Liu, Kaixiong Zhou, Fan Yang, Li Li, Rui Chen, and Xia Hu. Exact: Scalable graph neural networks training via extreme activation compression. In *International Conference on Learning Representations*, 2021.
- [22] Ayan Chakrabarti and Benjamin Moseley. Backprop with approximate activations for memory-efficient network training. *Advances in Neural Information Processing Systems*, 32, 2019.
- [23] R David Evans and Tor Aamodt. Ac-gc: Lossy activation compression with guaranteed convergence. *Advances in Neural Information Processing Systems*, 34:27434–27448, 2021.
- [24] Haohan Wang, Xindi Wu, Zeyi Huang, and Eric P Xing. High-frequency component helps explain the generalization of convolutional neural networks. In *Proceedings of the IEEE/CVF Conference on Computer Vision and Pattern Recognition*, pages 8684–8694, 2020.
- [25] K Ramamohan Rao and Ping Yip. *Discrete cosine transform: algorithms, advantages, applications*. Academic press, 2014.
- [26] Suyog Gupta, Ankur Agrawal, Kailash Gopalakrishnan, and Pritish Narayanan. Deep learning with limited numerical precision. In *International conference on machine learning*, pages 1737–1746. PMLR, 2015.
- [27] Alex Krizhevsky, Geoffrey Hinton, et al. Learning multiple layers of features from tiny images. 2009.
- [28] Chien-Chin Huang, Gu Jin, and Jinyang Li. Swapadvisor: Pushing deep learning beyond the gpu memory limit via smart swapping. In *Proceedings of the Twenty-Fifth International Conference on Architectural Support for Programming Languages and Operating Systems*, pages 1341–1355, 2020.

Appendix

A Proof of Theorem 1

Theorem 1. For any real-valued function $f(x)$ and its moving average $\bar{f}(x) = \frac{1}{2B} \int_x^{x+2B} f(t)dt$, let $F(\omega)$ and $\bar{F}(\omega)$ denote the Fourier transformation of $f(x)$ and $\bar{f}(x)$, respectively. Generally, we have $\bar{F}(\omega) = H(\omega)F(\omega)$, where $|H(\omega)| = \left| \frac{\sin \omega B}{\omega B} \right|$; and i denotes the imaginary unit.

Proof. We adopt the limit operator to reformulate $\bar{f}(x)$ into

$$\bar{f}(x) = \frac{1}{2B} \int_x^{x+2B} f(t)dt = \frac{1}{2B} \lim_{N \rightarrow \infty} \sum_{n=0}^{N-1} \frac{2B}{N} f\left(x + \frac{2Bn}{N}\right) = \lim_{N \rightarrow \infty} \sum_{n=0}^{N-1} \frac{1}{N} f\left(x + \frac{2Bn}{N}\right) \quad (9)$$

Taking Equation (9) into the Fourier Transform of $\bar{f}(x)$, we have

$$\begin{aligned} F'(\omega) &= \int_{-\infty}^{\infty} \bar{f}(x) e^{-i\omega x} dx = \int_{-\infty}^{\infty} \frac{1}{N} \lim_{N \rightarrow \infty} \sum_{n=0}^{N-1} f\left(x + \frac{2Bn}{N}\right) e^{-i\omega x} dx \\ &= \lim_{N \rightarrow \infty} \frac{1}{N} \sum_{n=0}^{N-1} \int_{-\infty}^{\infty} f\left(x + \frac{2Bn}{N}\right) e^{-i\omega x} dx \\ &= \lim_{N \rightarrow \infty} \frac{1}{N} \sum_{n=0}^{N-1} e^{i\omega \frac{2Bn}{N}} \int_{-\infty}^{\infty} f(x) e^{-i\omega x} dx = F(\omega) \lim_{N \rightarrow \infty} \frac{1}{N} \sum_{n=0}^{N-1} e^{i\omega \frac{2Bn}{N}} \\ &= F(\omega)(1 - e^{j\omega 2B}) \lim_{N \rightarrow \infty} \frac{1}{N(1 - e^{i\omega \frac{2B}{N}})} = F(\omega) \frac{1 - e^{j\omega 2B}}{-j\omega 2B} \end{aligned} \quad (10)$$

Let $H(\omega) = \frac{1-e^{j\omega 2B}}{-j\omega 2B}$. The magnitude of $H(\omega)$ is given by

$$\begin{aligned} |H(\omega)| &= \frac{|1 - \cos \omega 2B + i \sin \omega 2B|}{|\omega 2B|} = \frac{\sqrt{(1 - \cos \omega 2B)^2 + \sin^2 \omega 2B}}{|\omega 2B|} \\ &= \frac{\sqrt{4 \sin^4 \omega B + 4 \sin^2 \omega B \cos^2 \omega B}}{|\omega 2B|} = \frac{\sqrt{4 \sin^2 \omega B (\sin^2 \omega B + \cos^2 \omega B)}}{|\omega 2B|} \\ &= \left| \frac{\sin \omega B}{\omega B} \right| \end{aligned} \quad (11)$$

□

B Theoretical Compression Rate

We estimate the compression rate of DIVISION in this section.

Theorem 2. *The overall compression rate of DIVISION is given by $(B^{-2} + Q/32)^{-1}$, where B denotes the block-size of the moving average operation, and Q denotes the bit-width of the quantization.*

Proof. We first estimate the compression rate of each layer l , where $1 \leq l \leq L$; then give the overall compression rate during the training.

For each layer l of the model, DIVISION stores the tuple of $(\mathbf{H}_l^L, \mathbf{V}_l^H, \Delta_l, \delta_l)$ into the memory during the training. For the convenience of estimation but without loss of generality, the estimation of memory consumption is focused on the storage of the LFC \mathbf{H}_l^L and HFC \mathbf{V}_l^H for each layer l , because the scalar Δ_l and δ_l consumes far less memory than arrays \mathbf{H}_l^L and \mathbf{V}_l^H . Note that the LFC is given by $\mathbf{H}_l^L = \text{MeanFilter}(\mathbf{H}_l)$, where the block-size and moving stride of mean filtering are B . The LFC \mathbf{H}_l^L contains $B^{-2}N^2$ float numbers, which is $32B^{-2}N^2$ bits in total (32-bit per float number). Moreover, the HFC contains N^2 number, and each number is in Q -bit format. The HFC \mathbf{V}_l^H consumes N^2Q bits in total.

Considering the storage of both LFC \mathbf{H}_l^L and HFC \mathbf{V}_l^H during the training, the overall memory consumption is approximately $(32B^{-2} + Q)N^2$ bits, which is $(4B^{-2} + Q/8)N^2$ bytes (8-bit per byte). Note that the exact value of the activation map contains N^2 float numbers, which is $4N^2$ bytes (4-byte per float number). The compression rate R_{DIVISION} is given by

$$R_{\text{DIVISION}} = \frac{4N^2}{(4B^{-2} + Q/8)N^2} = \frac{1}{B^{-2} + Q/32} \quad (12)$$

Note that all layers have nearly the same compression rate. The overall compression rate of training the model is given by $(B^{-2} + Q/32)^{-1}$.

□

C Implementation details about DIVISION

DIVISION adopts block-size 8 ($B = 8$) and 2-bit quantization ($Q = 2$) to compress the activation maps of linear, convolutional and BatchNorm layers, where the compression rate is approximately 7.81%. For the operators without quantization error during backward propagation such as pooling layers, Relu activation, and Dropout, DIVISION follows the pipeline in Appendix C to compress the activation maps. For ActNN and DIVISION, we also adopt the *per-group quantization* [20] instead of the per-channel quantization for the compression to reduce the quantization variance. Other hyper-parameter settings are given in Table 3.

D Configuration of Baseline Methods

Existing work [22] has shown that BLPA requires at least 4-bit ACT for loss-less DNN training. We follow this setting for BLPA which has a nearly 12.5% compression rate for the inter-layer activation

Dataset	CIFAR-10	CIFAR-100	ImageNet	
Architecture	ResNet-18	DenseNet-121	ResNet-50	DenseNet-161
Epoch	100	200	120	90
Batch-size	256	128	256	256
Initial LR	0.1	0.1	0.1	0.1
LR scheduler	Cosine Annealing	Step LR	Cosine Annealing	Step LR
Weight-decay	0.0005	0.0005	0.0001	0.0001
Optimizer	SGD	SGD	SGD	SGD
SGD Momentum	0.9	0.9	0.9	0.9
Block-size B	8	8	8	8
Bit-width Q	2	2	2	2
Per-group Quant	256	256	256	256

Table 3: Hyper-parameter setting.

```

def forward(self, x: Tensor) -> Tensor:
    x = self.conv1(x)
    x = self.bn1(x)
    x = self.relu(x)
    x = self.maxpool(x)
    x = checkpoint.checkpoint(self.bottleneck_layer1, x)
    x = checkpoint.checkpoint(self.bottleneck_layer2, x)
    x = checkpoint.checkpoint(self.bottleneck_layer3, x)
    x = checkpoint.checkpoint(self.bottleneck_layer4, x)
    x = self.avgpool(x)
    x = torch.flatten(x, 1)
    x = self.fc(x)
    return x

```

Figure 5: Implementation of checkpointed ResNet-50 and WRN-50-2.

maps. AC-GC follows existing work [23] to take the multiplicative error $(1 + e_{AC-GC}^2) = 1.5$, where the searched bit-width enables AC-GC to satisfy this loss bound (training loss not more than 150% of vanilla training). In this setting, AC-GC finalizes the bit-width as 7.01 after the searching, which has a nearly 21.9% compression rate for the inter-layer activation maps. ActNN adopts 2-bit ACT and dynamic programming for searching the optimal bit-width specific for each layer, which has approximately 6.25% compression rate for the inter-layer activation maps. Such experimentally setting is denoted as L3 strategy in the original work [20], and we follow this setting in this section. Checkpoint relies on model-specific design of the checkpointed layers. We find that it provides good trade-off between memory consumption and running speed to checkpoint the first layer of each Bottleneck block in ResNet-50 and WRN-50-2. The forward function of our implemented ResNet-50 and WRN-50-2 is given in Figure 5. For the SWAP method, the memory utilization is considered both GPU and CPU because the caching involves both GPU and CPU in SWAP.

E Details about the Computation Infrastructure

The details about our physical computing infrastructure for testing the training memory footprint and throughput are given in Table 4.

Table 4: Computing infrastructure for the experiments.

Device Attribute	Value
Computing infrastructure	GPU
GPU model	Nvidia-A40
GPU number	1
GPU Memory	46068 MB